



Geophysical evidence of mantle upwelling associated with slab tearing below Central Greece: Geodynamical implications

Clarisse Kercet^{a,1}, Christel Tiberi^{a,*²}, Frédéric Gueydan^{a,3}, Rodolphe Cattin^{a,4}, Eleni Karagianni^{b,5}

^a Géosciences Montpellier, Université de Montpellier, CNRS, 34095 Montpellier, France

^b School of Geology, Aristotle University of Thessaloniki, Thessaloniki, Greece

ARTICLE INFO

Keywords:
Geophysics
Subduction
Extension
Aegean domain
Slab tearing
Mantle process

ABSTRACT

The tectonic evolution of the eastern Mediterranean region is largely influenced by two geological processes: subduction along the Hellenic arc and the westward extrusion of the Anatolian plate via the North Anatolian Fault. The interaction between these features, particularly at the termination of the North Anatolian Fault, has been widely studied but remains debated, largely due to the uncertain geometry of the African slab in the westernmost Hellenic arc. Here, we combined seismological and gravity datasets, revealing a complex deformation zone characterized by slab tearing, fault termination, and mantle upwelling. We processed two receiver function profiles, each about 500 km long and oriented perpendicular to the Hellenic trench, framing the southern tip of the North Anatolian Fault. These profiles reveal new slab geometry consistent with recorded seismicity, confirming slab break-off propagation. However, slab tearing alone cannot account for the regional mantle gravity field. Our findings indicate that asthenospheric upwelling at the slab tear location is necessary to explain the observed asymmetrical and bimodal gravity anomaly, coinciding with the North Anatolian Fault's termination and elevated surface heat flow. These insights enhance our understanding of deformation mechanisms in central Greece, suggesting that the slab tearing may have facilitated recent north-south extension in the Corinth rift, while asthenospheric flow concentrated strike-slip deformation on the North Anatolian Fault.

1. Introduction

The Aegean domain is the Europe's most seismically active region, characterized by a complex interplay of tectonic forces (e.g., Papazachos, 1990; Taymaz et al., 1990; Hatzfeld, 1999; Yolsal-Çevikbilen and Taymaz, 2012). This dynamic area has evolved through successive and cumulative deformations driven by the intricate interactions between the African, Eurasian, and Anatolian plates (Fig. 1, Taymaz et al., 1991; Gautier et al., 1999; Reilinger et al., 2010; Hollenstein et al., 2008; Pérouse et al., 2012). Two major geological processes drive the deformation: the westward extrusion of the Anatolian plate and the subduction along the Hellenic arc, leading to dextral strike-slip faults and

extensional basins (e.g. Le Pichon and Angelier, 1979; Lundgren et al., 1998; Armijo et al., 1999; Sengör et al., 2005; Papanikolaou and Royden, 2007).

While North Anatolian Fault ("NAF" Fig. 1) has accommodated most of the western extrusion of Anatolia in the past 15 Ma (Sengör, 1979; Le Pichon et al., 2003; Rodriguez et al., 2023), extension in the Aegean domain is more spatially and temporally distributed (Le Pichon and Angelier, 1979; Brun et al., 2016; Sternai et al., 2014). The onset of Aegean extension began 45 Ma ago (Brun and Sokoutis, 2010; Papanikolaou, 2013), driven by the rollback of the African slab (Royden, 1993; Jolivet and Faccenna, 2000; Brun and Faccenna, 2008; Durand et al., 2014). This process has accommodated up to 600 km of trench retreat

* Corresponding author.

E-mail addresses: clarisse.kercet@umontpellier.fr (C. Kercet), christel.tiberi@umontpellier.fr (C. Tiberi), frederic.gueydan@umontpellier.fr (F. Gueydan), rodolphe.cattin@umontpellier.fr (R. Cattin), elkarag@geo.auth.gr (E. Karagianni).

¹ ORCID: 0009-0002-3496-3609

² ORCID: 0000-0002-2302-3294

³ ORCID: 0000-0002-3369-7858

⁴ ORCID: 0000-0002-9825-9568

⁵ ORCID: 0000-0002-9268-2680

(Jolivet and Brun, 2010). From the Middle Eocene to the Middle Miocene, this back-arc extension is associated with the formation of Metamorphic Core Complexes in the central Aegean Sea through low-angle detachment systems (e.g., Brun et al., 2016; Brun and Sokoutis, 2018). Accelerating the trench retreat in the Middle Miocene changed the deformation pattern, promoting the development of extensional basins and high-angle normal faults distributed throughout the Aegean domain (e.g., Brun et al., 2016). Over the past 5 million years, the strain rate in the Aegean region has evolved towards a more localized deformation regime, potentially due to a Plio-Quaternary kinematic reorganization influenced by the activity of the NAF (Pérouse et al., 2012; Faucher et al., 2021). The NAF is thought to have entered the Aegean extensional domain at that time, and begun interacting with it (Armijo et al., 1996; Flérit et al., 2004; Ferentinos et al., 2018). The deformation has migrated from the central Aegean domain to its periphery, particularly concentrated in the Central Hellenic Shear Zone ("CHSZ" Fig. 1), at the western end of the Hellenic subduction zone and the termination of the NAF (Papanikolaou and Royden, 2007; Royden and Papanikolaou, 2011). This zone marks a diffuse boundary between Anatolia and Eurasian plates (Fig. 1), encompassing the Corinth and Evvia rifts system, where part of the extension is accommodated through NW-SE normal faults since 1–2 Ma (Armijo et al., 1996; Briole et al., 2021), with the emergence of E-W normal faults more recently (Faucher et al., 2021).

Some studies suggest that the CHSZ could be associated with a slab tearing at depth, resulting from a change in the nature of the subducting panel from continental lithosphere in the north to an oceanic lithosphere in the south (Royden and Papanikolaou, 2011; Jolivet et al., 2013). The entire Eastern Mediterranean system has experienced slab tearing in several locations. Tomographic studies reveal low-velocity mantle anomalies that indicate fragmentation of the African slab due to lateral changes in trench rates or lithospheric nature (Çubuk-Sabuncu et al., 2017; Biryol et al., 2011; Salatiñ et al., 2012; Govers and Fichtner, 2016; Portner et al., 2018). Thermal anomalies and volcanism are also reported in western Anatolia (Roche et al., 2019; Sengör et al., 2003) and in western Hellenic subduction zone (Fytikas and Kolios, 1979; Tzanis et al., 2022), which may also reflect the impact of rollback and tearing of the slab. Mantle flow through the tear and around the slab has been invoked to explain the lateral variations observed in the mantle seismic anisotropy in the East Mediterranean zone (Jolivet et al., 2015; Confal et al., 2020; Erman et al., 2025).

However, despite numerous studies, consensus on the geometry and nature of the African slab remains elusive. Challenges persist in reconciling complex observations with incomplete and sparse datasets. The number of tears, their location, shape and starting time are still a matter of debate (Faccenna et al., 2003; Biryol et al., 2011; Bocchini et al., 2018; Portner et al., 2018; Gürer et al., 2018). For the western Hellenic part, some models propose a smooth and continuous transition between

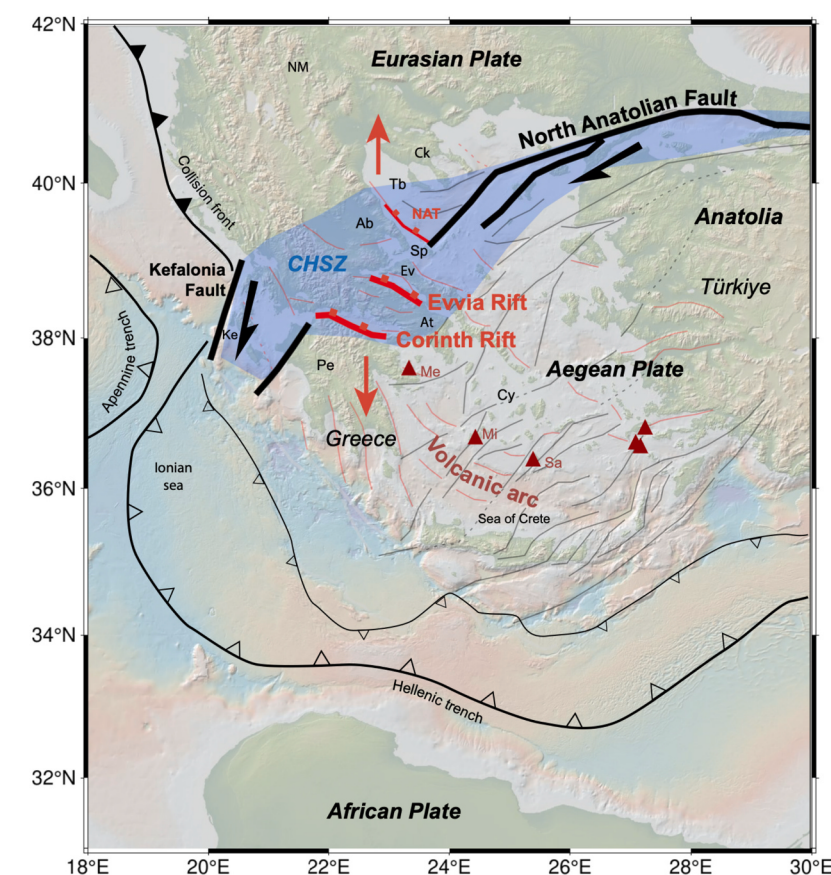


Fig. 1. Geodynamical setting and tectonic map of the Aegean region showing the main active structures and plates. The black line marked with open triangles corresponds to subduction zones, while the black line with filled triangles corresponds to collision zones. Major faults from Sakellariou and Tsampouraki-Kraounaki (2018) and Gueydan et al. (2025): normal faults are shown as thin red lines, and strike-slip faults as thin grey lines. Dashed grey lines display potential fault extensions. Corinth and Evvia rifts locations are indicated as thick red lines. The thick black lines represent major faults, such as the North Anatolian Fault and the Kefalonia Fault. Main volcanic arc edifices (red triangles) are indicated (Me: Methana; Mi: Milos; Sa: Santorini). Ck: Chalkidia; NM: North Macedonia; At: Attica; Cy: Cyclades Islands; Ab: Almiros basin; Ev: Evvia Islands; Sp: Sporades basin; Pe: Peloponnesus; Th: Thermaikos basin; Ke: Kefalonia; NAT: North Aegean Trough; CHSZ: Central Hellenic Shear Zone (blue zone as defined in Papanikolaou and Royden, 2007 and Royden and Papanikolaou, 2011). (For interpretation of the references to colour in this figure legend, the reader is referred to the web version of this article.)

continent and oceanic lithosphere (Halpaap et al., 2018; Olive et al., 2014; Grigoriadis et al., 2016; Evangelidis, 2017; Bocchini et al., 2018; Kassaras et al., 2020a), while others argue for a discontinuous and torn slab, either vertical (Royden and Papanikolaou, 2011; Suckale et al., 2009; Pearce et al., 2012) or trench parallel (Wortel and Spakman, 2000; Hansen et al., 2019). Regional reconstructions based on geological observations and seismic tomographic images suggest the presence of hot mantle flow associated with slab tears (Jolivet et al., 2015; Evangelidis, 2017; Rappisi et al., 2025). However, the limited information regarding the exact shape of the tears, makes it difficult to predict the associated flow and its effects on the Aegean lithosphere, as well as its interaction with pre-existing tectonic structures.

Determining the geometry of the African slab in the western part of the Hellenic subduction zone is crucial for assessing its effect on surface deformation. This region, characterized by the highest extension rates in Europe, and significant interactions between major active tectonic features, requires a clear understanding of how slab geometry relates to the CHSZ and the termination of the NAF (Guillaume et al., 2013). To address this issue, we propose to define the slab geometry in its western part through mantle density models constrained by seismic observations. Receiver functions and the distribution of instrumental seismicity will first help us identify any discontinuous patterns in the structures. We will then integrate this information with the long-wavelength resolution of gravimetry in our density models. Next, we will test the gravity signature of three slab models: continuous, discontinuous, and a discontinuous model with a mantle window. Finally, we will discuss the geodynamic implications of our results, with a specific focus on the interaction between mantle structures and surface deformation.

2. Data

The presence of water-covered areas in central Greece, extending from the Hellenic trench to the Aegean Sea coastline (Fig. 1), presents challenges for installing seismic stations and affects the spatial resolution of seismic models. However, gravimetry overcomes this limitation by offering continuous data collection through satellite missions, as well as land and marine surveys. In the study area, gravity measurements have mainly been used to characterize the crust, particularly focusing on its thickness (e.g. Tirel et al., 2004; Grigoriadis et al., 2016; Makris et al., 2013; Chailas et al., 2021; Chailas et al., 2022). As a result, the authors have largely avoided exploring longer wavelengths associated with the mantle, especially concerning the African slab, by relying instead on tomographic models.

In this work, we adopt an alternative approach by using the long-wavelength component of seismological and gravity data to explore deeper geological structures. The datasets cover the entire Hellenic arc spanning from 19° to 30° in longitude and 35° to 42° in latitude. We do not rely on the velocity-density transition laws commonly used to convert tomographic models into density models. Instead, we prioritize the long-wavelength signal from an available global gravity model, which provides greater spatial continuity than tomographic models limited by the station coverage and ray path distribution.

2.1. Seismological data

We use two types of seismological data for our analysis. The first type consists of the local seismicity distribution, which allows us to localize disruptive patterns and to identify discontinuous behaviours in the area, as already investigated in this highly seismic zone (e.g. Bocchini et al., 2018; Kassaras et al., 2020a). Previous studies have extensively examined the seismicity distribution in the Aegean area (e.g. Makropoulos and Burton, 1981; Hatzfeld, 1994; Papazachos et al., 2000; Meier et al., 2004; Sachpazi et al., 2016). In this study, we aim to focus on the western end of the subduction zone to gain insights into potentially disrupted areas that can guide our direct gravity modelling. We use the global catalogue from the reviewed International Seismological Centre

Bulletin (Engdahl et al., 1998) which contains instrumental seismicity between 1964 and 2023. Since our study is focused on the upper mantle, we restrict our research to events at depths greater than 40 km in the western Hellenic area. The associated output is made of 4662 events with magnitudes ranging between 2 and 6.5 (Fig. 2).

The second type of seismological data is for receiver functions (RF) processing and the associated migration profiles. This dataset is obtained from NOA and IRIS data centres, with a sampling rate of 100 samples per second (supplementary material T1). It includes three-component seismograms from 21 stations of the National Seismological Network of Greece (FDSN codes HA, HL, HP and HT), managed by the Hellenic Unified Seismological Network at the University of Athens, covering the years 2010 to 2024. Additionally, we supplement this dataset with information from the MEDUSA project, which operated between 2006 and 2007 (FDSN code XS, Rondenay, 2006, supplementary material S1). For our analysis, we select teleseismic events with epicentral distances between 30° and 90° and magnitudes greater than 6.5. The signals are filtered within the frequency range of 0.08 to 0.8 Hz and are limited to 15 s before and 40 s after the first P-wave arrival, as classically processed (e.g. Sodoudi et al., 2006; Cossette et al., 2016).

2.2. Gravity information

We use the global Earth Gravity Model (EGM2008), which combines terrestrial, altimetry-derived, airborne, and satellite gravity data (Pavlis et al., 2008). The complete Bouguer anomaly is obtained on a 2.5 arc-minute grid by computing the topographic effect from Fullea et al. (2008), using a density reduction of 2670 kg.m⁻³ and 1 arc-minute grid ETOPO1 Digital Elevation Model (Fig. 3a and supplementary material S2).

3. Methods

We gather insights from three different datasets: the intermediate-depth seismicity distribution from the reviewed ISC catalogue, the teleseismic waveforms, and the gravity signal. Each dataset is processed independently, and the results are later combined in our direct gravity modelling approach.

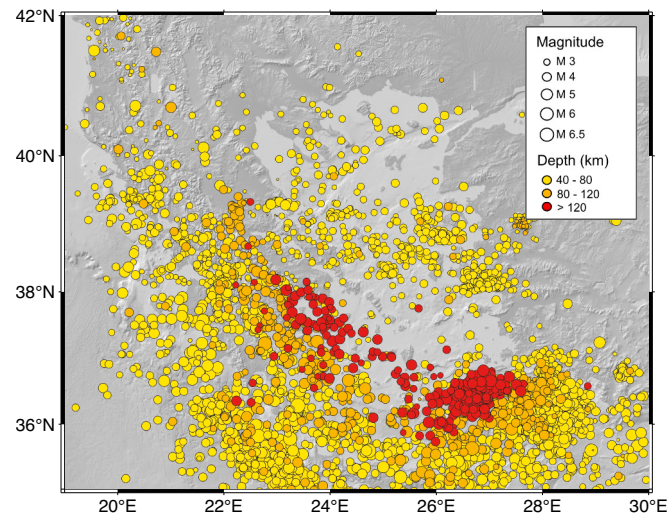


Fig. 2. Topographic and bathymetric map of the study area showing the location of the seismic events from 40 km down to 281 km depth, from the reviewed International Seismological Centre Bulletin (Engdahl et al., 1998). The yellow circles correspond to events between 40 and 80 km depth. The orange circles correspond to events between 80 and 120 km depth, and the red circles to those deeper than 120 km. The total number of events plotted is 4662. (For interpretation of the references to colour in this figure legend, the reader is referred to the web version of this article.)

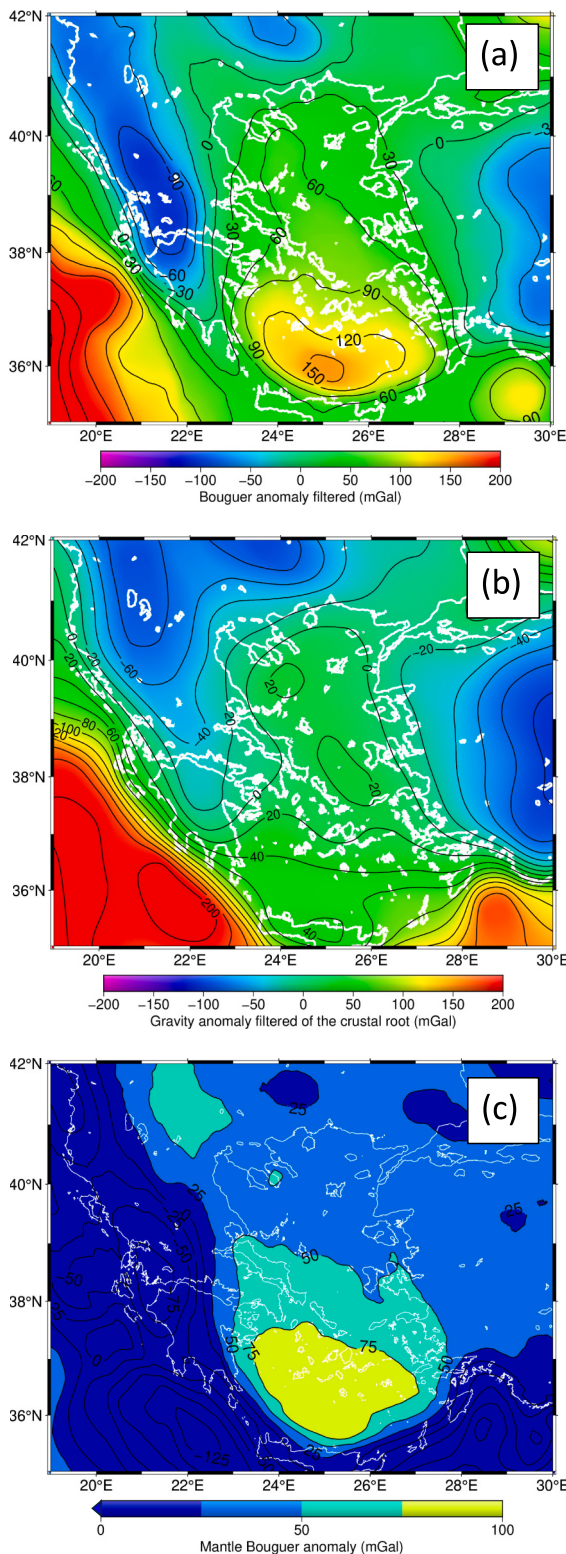


Fig. 3. Gravity anomaly maps of the Aegean region. (a) EGM2008 complete Bouguer (100 km-low-pass filtered), (b) gravity signal of the isostatic root effect (100 km-low-pass filtered), and (c) associated Mantle Bouguer Anomaly (MBA).

First, we process the teleseismic data to calculate the RFs along two profiles. Next, we work on the complete Bouguer anomaly to isolate the mantle signal, referred to as the Mantle Bouguer Anomaly (MBA).

Finally, we use the intermediate-depth seismicity distribution and the RF signal to constrain direct density models and calculate their

associated gravity signal. The synthetic outputs are then compared with the observed MBA to identify the best-fitting model.

3.1. Receiver functions

We calculate the RFs through an iterative time-domain deconvolution to remove the source and instrumental responses (Ligorria and Ammon, 1999). Prior to the deconvolution, we rotate the three components of the seismogram from a geographical (Vertical - North - East) to LQT (P-Sv-Sh) coordinate system. We use the event theoretical ray parameter and backazimuth to optimize the energy of the converted Ps wave on the radial (Q) component. We process the deconvolution through 200 iterations with a Gaussian width filter of 2.5 s. We then select the obtained RF with a reproduction rate greater than 85 %, and we visually inspect the signal to remove potential outliers (supplementary material S3). The resulting 1215 quality-controlled RF are time-to-depth migrated along two profiles using IASP91 velocity model (Kennett and Engdahl, 1991). This is done by backtracing the ray paths of the Q component from the station elevation down to 160 km depth using the common conversion point (CCP) stacking technique (Yuan et al., 1997; Subedi et al., 2018; Michailos et al., 2023). This technique is particularly suitable for testing the continuity of horizontal or sub-horizontal impedance contrasts.

3.2. Mantle Bouguer anomaly

The complete Bouguer anomaly derived from EGM2008 contains signals from both crustal and mantle sources. We applied a 100 km low-pass filter to remove the shortest wavelengths, which originate solely from crustal sources and potential aliasing in the EGM2008 data (Fig. 3a). The resulting filtered Bouguer anomaly is very similar and consistent with previous gravity maps obtained from interpolated ground observations (Lagios et al., 1996; Grigoriadis et al., 2016; Kasaras et al., 2020b).

To isolate the mantle signal, we remove the crustal effects through a series of corrections to obtain the Mantle Bouguer Anomaly (MBA). These corrections are calculated over a wide area, spanning longitudes from 14° to 35° and latitudes from 30° to 47°, to prevent edge effects from influencing the study area. First, we calculate the gravity effect of an isostatic crustal root. We compute the crustal thickness of the region (supplementary material S4), assuming a local compensation for the topography (Tirel et al., 2004; Suckale et al., 2009; Pearce et al., 2012; Makris et al., 2013). We assume a density contrast of 600 kg.m⁻³ between the crust and the mantle, a density of 1035 kg.m⁻³ for the seawater, and a mean crustal thickness of 30 km (Tirel et al., 2004; Grigoriadis et al., 2016). The corresponding gravity signal is then calculated with a Python code using the Harmonica library, developed through a three-dimensional distribution of prisms that samples the volume between the crustal topographic root surface and the compensation depth. We compute the gravity effect on a regular grid of 6 arc minutes. This Python code has been modified from an original code designed to compute the gravitational effect of topography and is part of the Fatiando a Terra Project (Uieda et al., 2013; Uieda and Barbosa, 2017). The resulting gravity signal (see supplementary material S5) is then filtered with a 100 km low-pass filter, likewise the complete Bouguer anomaly, and ranges between -100 and 200 mGal for our study area (Fig. 3b).

The obtained MBA ranges from -125 to ca. 100 mGal, with the maximum value localized in the Cyclades (“Cy” Fig. 1) and Sea of Crete (Fig. 3c). A secondary maximum is localized north of 40° latitude, near North Macedonia (noted “NM” Fig. 1). The negative values in the Ionian Sea are due to the oceanic nature of the crust in this area that we do not include in our calculation. This signal will not be discussed further, as the focus of this article is on the deep part of the slab in the Aegean Sea, which is unaffected by this anomaly.

3.3. Three-dimensional gravity model

Finally, we employ the Matlab code GEEC (Gal Eötvös Earth Calculator) developed by Saraswati et al. (2019) to test various model geometries for the African slab in the Aegean region. Based on the analytical solutions of expanding the line integrals of a constant-density polyhedron body and considering the curvature of the Earth, this code computes the gravity field due to irregularly shaped body mass. We assume a constant density contrast of 100 kg.m^{-3} between the Aegean mantle and the subducting slab, and -50 kg.m^{-3} between the asthenosphere and the slab. We consider a constant slab thickness of 100 km, extending from 80 km to 200 km depth.

We use information derived from seismological data (seismic catalogues and our seismic results) to constrain the density models and testing hypotheses regarding the shape of the African slab. We use an iterative modelling approach, gradually increasing the complexity of the model to better align with the observed MBA signal.

4. Results

4.1. Seismological constraints

The distribution of the intermediate-depth seismicity (depth > 80 km, Fig. 4) reveals that seismicity occurring deeper than 120 km depth does not display the same continuous distribution as that observed between 80 and 120 km depth. No instrumental seismicity is observed below 120 km north of Attica and Evia ("At" and "Ev" Fig. 1). The station VILL marks the northern limit of deep seismicity (> 120 km), emphasised by a blue dashed line Fig. 4. This pattern, also mentioned by Bocchini et al. (2018) and Kassaras et al. (2020b), can be used as seismicity inferred boundaries for the slab geometry.

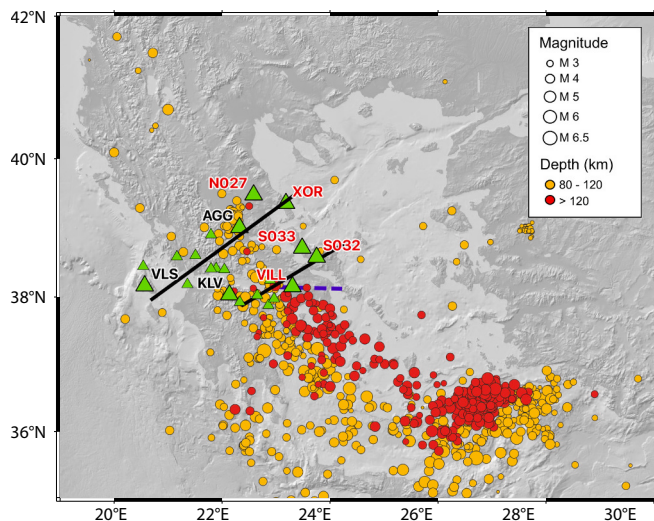


Fig. 4. Topographic and bathymetric map of the study area showing the location of the seismic events from 80 km down to 281 km depth, from the reviewed International Seismological Centre Bulletin (Engdahl et al., 1998). The orange circles correspond to events between 80 and 120 km depth, and the red circles to those deeper than 120 km. The total number of events plotted is 1114. Green triangles give the location of seismic stations used to calculate the receiver functions. Stations aiding the interpretation of the two migrations (profiles in black lines) are labelled and marked with larger triangles to facilitate their identification. The remaining stations used are listed in the supplementary materials T1 and S1. Stations showing mantle low-velocity zones (LVZ) in the receiver functions below approximately 60 km are shown in red for better interpretation. The thick dashed blue line at station VILL indicates the northern end of the deep seismicity (>120 km). (For interpretation of the references to colour in this figure legend, the reader is referred to the web version of this article.)

We migrate the RFs along two 500-km long SW-NE profiles, roughly perpendicular to the Hellenic trench, and framing the southern tip of the NAF (Fig. 4). The northern profile (Fig. 5a) extends from Kefalonia ("Ke" Fig. 1) up to North Aegean Trough, while the southern profile (Fig. 5b) spans from Peloponnesus ("Pe" Fig. 1) up to Sporades Island ("Sp" Fig. 1). The Aegean Moho and the African slab Moho are delineated by positive impedance contrast with depth, whereas the top of the African slab exhibits a negative contrast due to the lower seismic velocity of the oceanic crust compared to the surrounding Aegean mantle (outlined by the black continuous line, Fig. 5). The RFs yield an average Aegean Moho depth that closely matches the isostatic prediction (Fig. 5a and b), a posteriori validating the hypothesis made for the MBA calculation, and aligning with previous observations on 2D profiles (Pearce et al., 2012; Ranjan and Konstantinou, 2024).

In both profiles, the slab signature is coherent with the Wadati-Benioff zone of seismicity (Fig. 5). The end of the seismicity between AGG and N027 for the northern profile and between PROD and VILL for the southern one, coincides with the end of the RF seismic signature of the slab. The top of the slab reaches depths of 70–90 km at these locations, coherent with the former results of Suckale et al. (2009). This disruption in the slab signature concurs with thick negative RF amplitudes at ca. 50–60 km depth beneath the north-eastern tip of the profiles (N027-XOR station for the northern profile and VILL-S033-S032 for the southern one, Fig. 5). These negative conversions indicate a decrease in seismic velocity with depth and correlate with the gap in the intermediate-depth seismicity (Fig. 4).

The abrupt stop in the RF signal and the gap in the intermediate-depth seismicity also coincide with the end of the volcanic arc in Methana (Vougioukalakis et al., 2019). This discontinuity observed in several signals concurs with the proposition of a slab tearing (Guillaume et al., 2013; Hansen et al., 2019; Suckale et al., 2019) and indicates the location of the southern edge of the tearing. The shape and extension of the tear remain ambiguous from these first images. Our seismological constraints indicate that the slab signature is still missing beneath the N027 station on the northern profile, and low velocity anomalies are present in the upper mantle, suggesting hotter material or an anomalous mantle where the slab signature is absent. This local observation is difficult to observe in the existing tomographic images, as the associated depth and lateral extension lie at the edges of tomographic resolution (Piromallo and Morelli, 2003; Hansen et al., 2019; Ranjan and Konstantinou, 2024).

Seismic signals, including earthquake distribution and RFs, reveal discontinuous patterns and low-velocity anomalies North of Evvia. These features may be related to variations and disruptions in the slab geometry. However, the uneven distribution of the seismic stations in this area, with distances exceeding 50 km between them in the Gulf of Evvia region, limits our ability to accurately determine the shape, location, and extent of the slab tearing, as well as the associated anomalous hot material. Taking advantage of the continuity and long-wavelengths of the MBA gravity signal, we collect continuous information over a broad area, overcoming the main limitation of the seismological approaches.

4.2. Gravity modelling

We first model a plain and continuous African slab to assess our parametrization and to serve as a reference. We base its geometry on previous geophysical studies (Tsokas and Hansen, 1997; Grigoriadis et al., 2016; Halpaap et al., 2018) and adjust it to account for our observation results. We infer the slab amphitheatrical shape (Fig. 6a) and dimensions from the distribution of the regional seismicity (Fig. 4), the shape of the volcanic arc (Fig. 1), and previous geophysical studies (Salaün et al., 2012; Bocchini et al., 2018; Halpaap et al., 2018). The resulting bean-shaped gravity anomaly displayed in Fig. 6d is very similar to the model of Grigoriadis et al. (2016). This anomaly extends from the south-eastern Aegean Sea, near the southern coast of Türkiye,

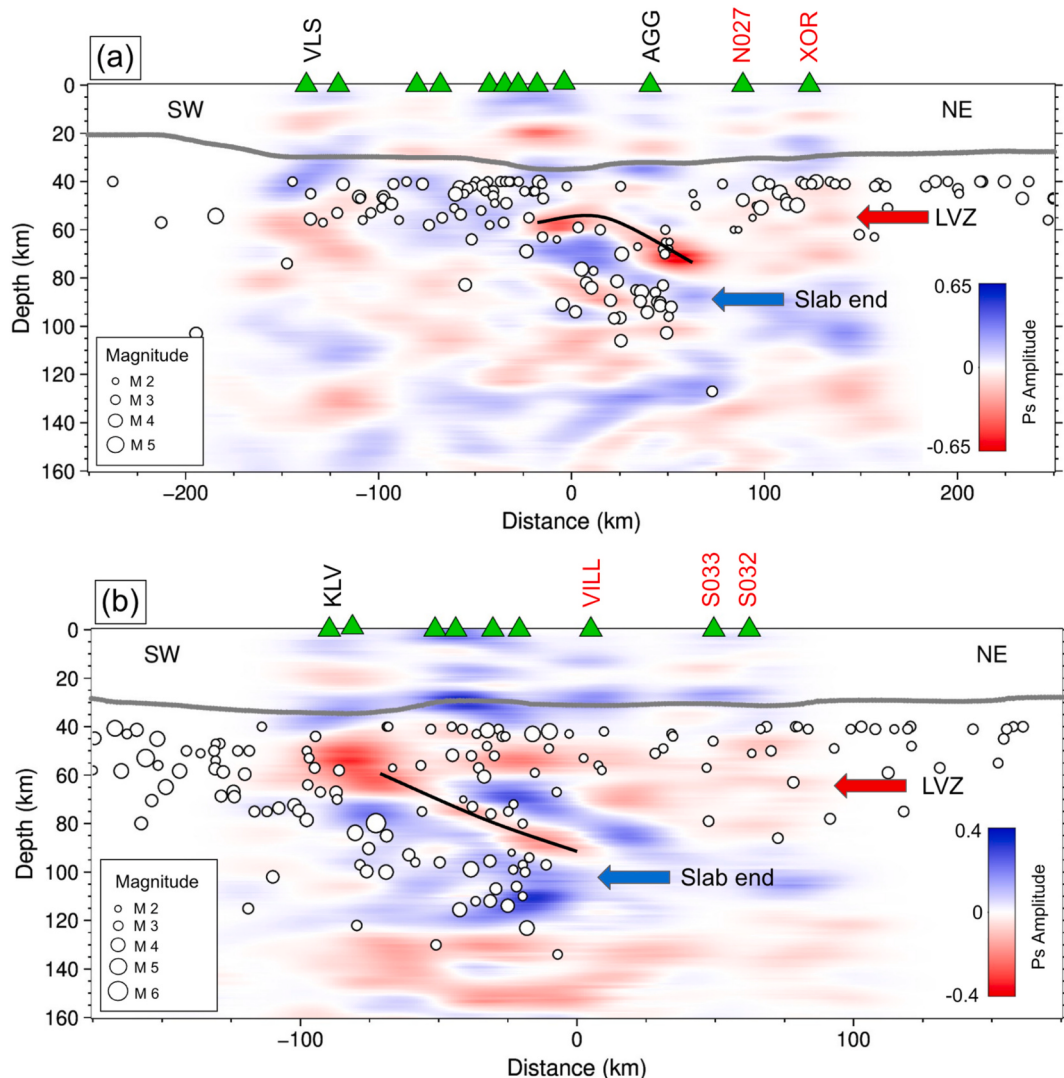


Fig. 5. (a) North and (b) south migration profiles obtained from receiver function analysis. Positive and negative impedance contrast with depth are associated with blue and red colour, respectively. Projected seismicity from 40 km depth from the reviewed International Seismological Centre Bulletin (Engdahl et al., 1998) is shown with white circles. The grey line represents the isostatic Moho calculated from the ETOPO1 grid. The slab top is highlighted with a black plain line. Stations displaying mantle low velocity zones (LVZ) below ca. 60 km are indicated in red. (For interpretation of the references to colour in this figure legend, the reader is referred to the web version of this article.)

to the northeast of Evvia Gulf (Almiros basin noted “Ab” Fig. 1). Our model exhibits a maximum amplitude of 90 mGal, higher than the 65 mGal reported by Grigoriadis et al. (2016) (Fig. 6d). Besides, it features a maximum that is shifted northeast, providing a better fit to the observed MBA. However, while our obtained anomaly corresponds in amplitude to the observed MBA, it fails to explain the asymmetrical shape of the mantle gravimetric signal. The MBA is discontinuous with two distinct high values, one above the Cyclades and another above North Macedonia (Fig. 3c). A continuous slab cannot explain the decrease in MBA above the Thermaikos basin (“Tb” Fig. 1) (> 25 mGal), indicating the need for a more complex model that incorporates lateral density variations.

We design our second model to address the observed asymmetries, and test a vertical tearing in the slab that induces a density decrease (Fig. 6b). We set the spatial limits of the slab tearing from the seismicity distribution, our RF migration profiles, and previous tomographic and seismological works (Suckale et al., 2009; Salaün et al., 2012; Olive et al., 2014). We assume its vertical extends from 120 km down to 200 km as pinpointed by the gap in the deep seismicity (Fig. 4). We set the southern edge of the slab tearing near south Evvia, where the Aegean

volcanic arc ends (Vougioukalakis et al., 2019). The southern edge is roughly east-west oriented, to fit the end of the deep portion of the Wadati-Benioff zone (seismicity depth > 120 km depth, Fig. 4). Determining the northern edge of the tearing is more challenging due to sparse seismic observations. Recent seismological works on MEDUSA data inferred a continuous slab north of 40° (Pearce et al., 2012; Olive et al., 2014). We thus locate the tear near the Thermaikos and Almiros basins, south of Chalkidia (“Ck” Fig. 1), where the MBA displays its minimum value, and strong gradients in upper mantle seismic velocities are observed (Salaün et al., 2012; Halpaap et al., 2018). This discontinuous slab model generates an asymmetrical anomaly, which is more compatible with the observed MBA, with a single maximum centred in the Cyclades (Fig. 6e). The amplitude of the anomaly decreases by more than 20 mGal in Attica and Evvia. However, this model still fails to reproduce a distinct secondary maximum further north, indicating the need for further reduction in density.

We finally test a third model incorporating an asthenospheric body within the modelled slab tearing accounting for a lower density contrast (Fig. 6c). The upper limit of the asthenospheric body (60 km) exceeds the slab top (80 km), as indicated by our RF profiles and previous seismic

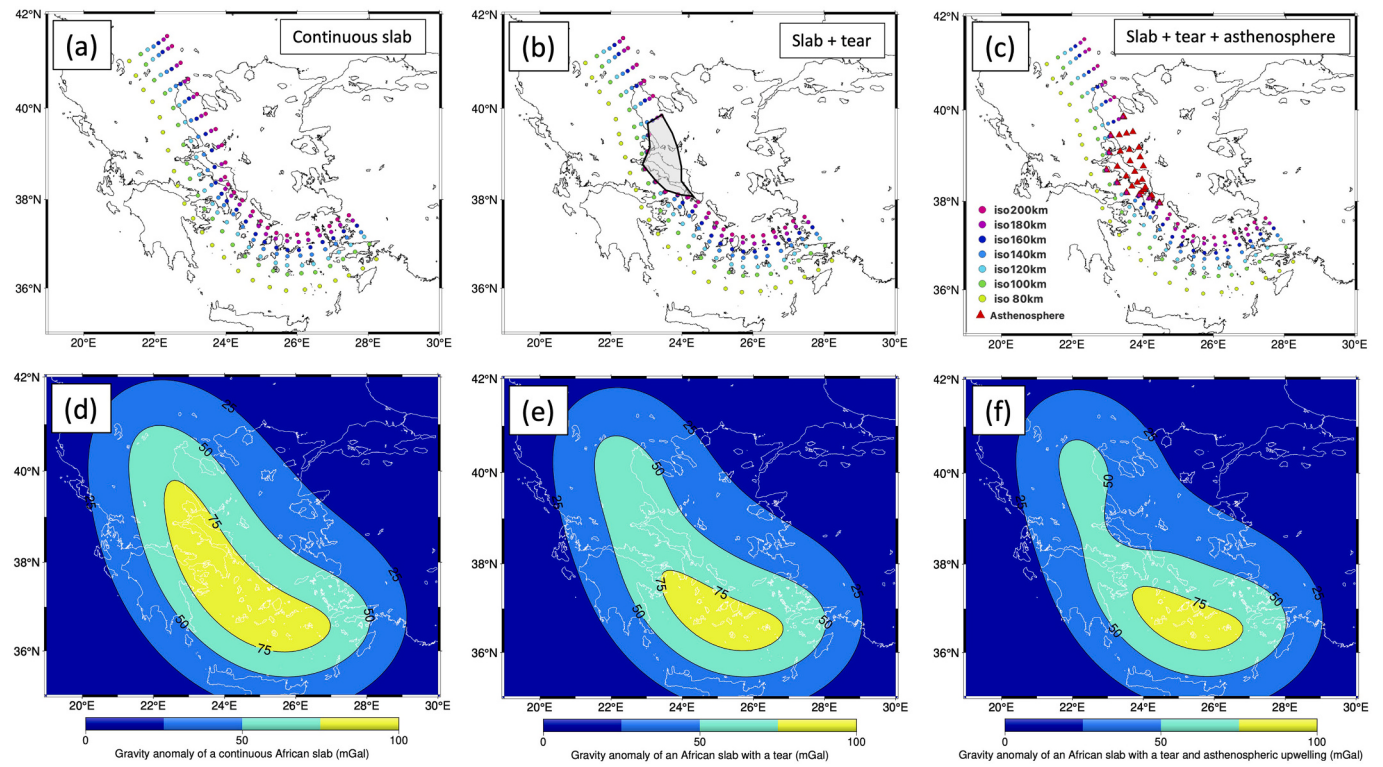


Fig. 6. Gravity effect of (a) a continuous slab, (b) a slab with a tear (grey shaded area), (c) a slab with a tear and an asthenospheric upwelling (red triangles). The upper row (a – c) gathers the map views of the model parametrisation, with only the depth of the top layer nodes (colour scale in c). The lower row (d – f) displays the gravity anomaly of the associated models. (For interpretation of the references to colour in this figure legend, the reader is referred to the web version of this article.)

tomography analysis (Halpaap et al., 2018). Both methods show a decrease in velocity at depths of 60–80 km. The resulting anomaly is more closely aligned with the observed MBA, featuring an absolute maximum restricted to the Southern Cyclades domain, and a more pronounced asymmetrical shape (Fig. 6f). By including a buoyant body within the slab tearing, we are able to reduce the northern part of the anomaly and introduce a secondary maximum located beneath North Macedonia and Almiros basin. While the geometry of our models does not perfectly match the observed MBA in all respects, particularly concerning the discontinuous shape of the MBA and the location of the secondary maximum, this model reveals the main factors that contribute to the first-order characteristics of the mantle gravity signal. Our models demonstrate that only a discontinuous slab with a narrow tearing associated with an asthenospheric upwelling is coherent with the observed deep gravity signature. We subsequently discuss the potential variations and adjustments required to better align our models with the observations.

5. Discussion

5.1. Validity of the proposed model

It is well-known that seismicity catalogues are not exhaustive, and the quality of the data is widely uneven, reflecting the use of 1D simplified models in global catalogues or dissimilar station coverage in space and time, among others. Numerous attempts exist to locate or relocate the Aegean seismicity (e.g. Makropoulos and Burton, 1981; Papazachos, 1990; Engdahl et al., 1998; Halpaap et al., 2018; Halpaap et al., 2019; Kassaras et al., 2020b; Ranjan and Konstantinou, 2024). Instead of mixing the catalogues without controlling their uncertainty and coherence, we favour the ISC database in the region, already used to characterize the Hellenic subduction and the Aegean lithosphere (Bocchini et al., 2018). We are fully aware that this catalogue, by neglecting the slab high-velocity anomaly, presents some bias (Meier

et al., 2004). The seismic activity extracted from other databases displays a disrupted pattern in the same area, which remains consistent with the interruption of the RF signal (U.S Geological Survey, 2025; Kassaras et al., 2020b; Supplementary material S6). Regardless of which catalogues we reference, the seismicity consistently identifies the same section of slab break.

It is well-established that the greater the number of mass bodies in a model, the better the fit with gravity data. Here, we adopt a parsimonious approach that balances model fit and simplicity, as advocated by Akaike (1974). Our direct modelling approach employs only two mass bodies - the African slab and upwelling mantle - to account for the calculated MBA, RF image, and seismicity location. We recognize that the simple model we propose is not the only possible alternative. Specifically, we associate the gravity long-wavelength component with mantle structures. However, long-wavelength signals can also originate from wide crustal bodies or regional Moho variations. Regional seismological studies display a smooth Moho in the North Anatolian trough and beneath the Thermaikos basin, which deepens towards the northwest (Ranjan and Konstantinou, 2024; Karagianni et al., 2005; Sodoudi et al., 2006). This feature is also observed in our isostatic Moho map (supplementary material S4c). This pattern does not align with the observed MBA, which depicts its secondary maximum in North Macedonia (Fig. 3c). While we cannot completely rule out the possibility that the Moho signature is still present in the MBA, it is deemed unlikely. Our latest model, which features a slab tear allowing for asthenospheric upwelling, effectively explains all geophysical data (seismological and gravimetric) in the region. Therefore, it should be considered a potential solution.

Our approach demonstrates that gravity observations are inconsistent with a continuous and smooth slab, as proposed in models solely based on seismological data (Pearce et al., 2012; Halpaap et al., 2019). If the first-order bean-shape of the MBA (Fig. 3c) is easily explained by the amphitheatrical-like shape of the Hellenic slab (Figs. 6a,d), a vertical tearing within the slab associated with an asthenospheric window is

necessary to reproduce the asymmetrical shape of the MBA, particularly its secondary maximum centred in North Macedonia (Fig. 3c). Previous authors have already suggested the presence of a tearing in the African slab, either with a southward horizontal propagation creating an asthenospheric flow (Wortel and Spakman, 2000; Hansen et al., 2019), or with a vertical shear delimiting the rapid subducting Ionian oceanic lithosphere from the slowly subducting Adriatic continental lithosphere (Suckale et al., 2009; Royden and Papanikolaou, 2011). The tearing's shape, location, and nature remain a matter of debate, as the sparsity and resolution of the data often allow for more than one potential model. Here, we propose that the slab tearing is vertical with an asthenospheric window allowing the deeper mantle to rise, which explains the first-order long-wavelength gravity signal (Figs. 6c,f). The southern edge of the slab breach is well-defined from the observed strong gravity gradient (Fig. 3c), and from several other independent observations (Olive et al., 2014; Vougioukalakis et al., 2019). In particular, it also coincides with SKS splitting null measurements in Evvia and Attica (Olive et al., 2014; Confal et al., 2020). The abrupt change in the anisotropic direction in this region can reflect the impact of mantle flow through the slab window, as observed beneath Türkiye (Confal et al., 2018). A null or weak

anisotropic anomaly can be attributed to a vertical mantle material flow (Ermann et al., 2025). However, the simplicity of our model does not fully reproduce the observed MBA shape, and several alternatives and modifications can be considered to match the observations better (Fig. 3c):

- The slab's real shape likely differs from our models' simplified architecture. In particular, the secondary maximum of the MBA, located beneath North Macedonia, is roughly 150 km further north than our modelling results. This suggests that our third model (Fig. 6c) is an end-member scenario with the narrowest tearing width, and the northern edge of the tearing could extend further north. The shape of the MBA, with this clear secondary maximum beneath North Macedonia confirms the presence of the slab in this region and rules out models with continuous trench parallel tearing (Wortel and Spakman, 2000; Hansen et al., 2019). Based on our results, we estimate the northern edge of the tearing to be located within the Sporades or Thermaikos basins.
- The asthenospheric upwelling inferred from RF results may be more complex than our designed vertical volume. A three-dimensional

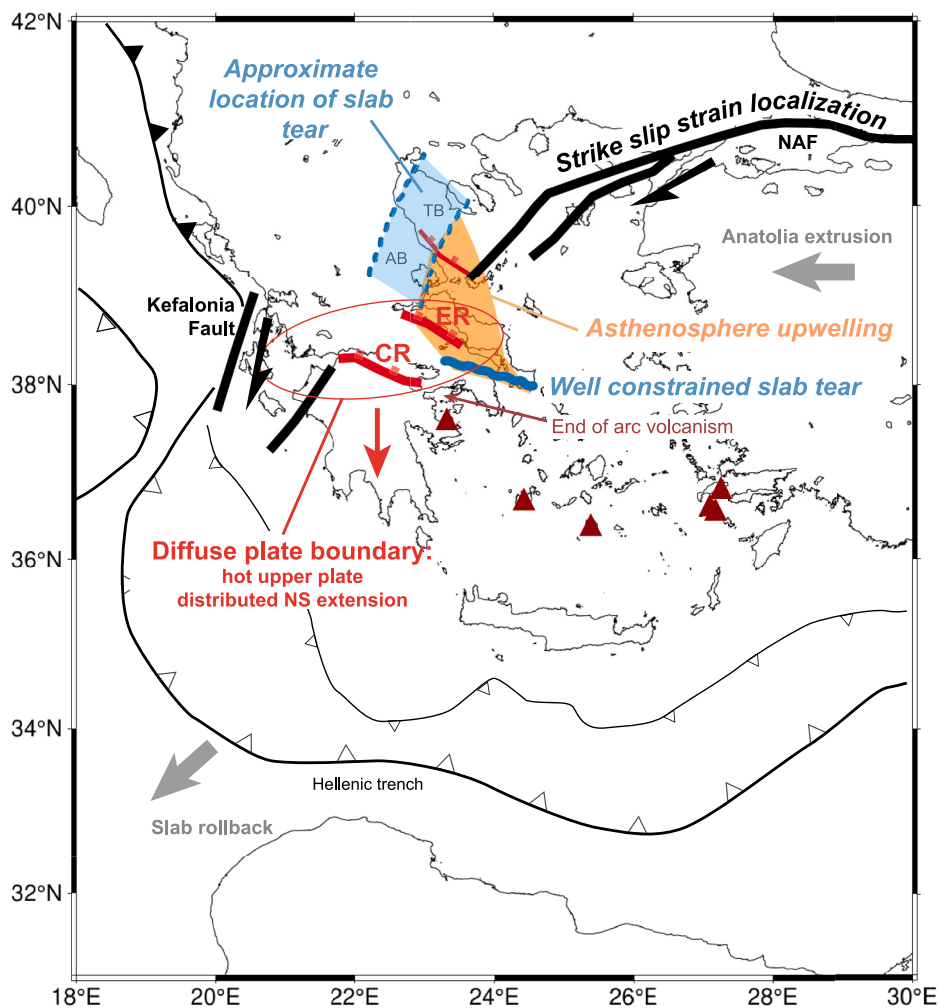


Fig. 7. Final interpretative scheme; CR: Corinth rift; ER: Evvia Rift; TB: Thermaikos basin; AB: Almiros basin. The slab rollback and the extrusion of Anatolia have induced distributed deformation through the whole Aegean domain since the Miocene. This deformation is accommodated by both strike-slip and normal faults. The tearing of the African slab begins at a depth of 100–120 km beneath the Evvia and Thermaikos basin (the blue lines represent the edges of the tear). This process intensifies the extension in the region in a north-south direction and promotes a distributed extensional system through the Corinth and Evvia rifts system (CR, ER). The slab breach enables a low-density asthenospheric upwelling to propagate up to a depth of ~60 km (indicated by the orange-shaded area), and the associated thermal anomaly facilitates the localization of strike-slip strain along the North Anatolian Fault (NAF), pulling its western tip to the southwest. (For interpretation of the references to colour in this figure legend, the reader is referred to the web version of this article.)

shape with a lateral spreading head above the slab top (at 80 km depth) is plausible. In this case, the modelled anomaly would likely be closer to the observed MBA, with a low amplitude beneath North Aegean Trough due to the proximal buoyant source.

- All our models are density-dependent, and considering a heterogeneous density distribution could improve the fit. Especially in our study zone, where changes in the nature and buoyancy of the African slab are expected (Baker et al., 1997; Royden and Papanikolaou, 2011).

5.2. Geodynamical implications

Our study refines the location and shape of the African slab tearing and identifies a zone of asthenospheric upwelling (Figs. 6c and 7). The slab tearing is bounded to the south by the Corinth rift area and Attica, and to the north by the Almiros and Thermaikos basins. The associated asthenospheric upwelling is located beneath Evvia Island and includes the termination of the NAF. Their location concurs with high seismic attenuation in the range of 40–100 km depth (Hashida et al., 1988; Ranjan and Stehly, 2024), high heat flow (Fytikas and Kolios, 1979; Stiros, 1991; Cloetingh et al., 2010) and low electrical resistivity (Galanopoulos et al., 2005). The existence of hot springs, Quaternary volcanism, and consequent fraction of Mantle-He in hydrothermal fluids in northern Evvia Island are coherent with a perturbed geotherm due to a shallow asthenospheric window (Pe-Piper and Piper, 2007; Pik and Marty, 2009). The southern limit of the asthenospheric upwelling is marked by the north-western end of the Aegean volcanic arc in the Methana peninsula, which signs the end of the slab-related volcanism (Pe-Piper and Piper, 2005; D'Alessandro et al., 2008, Fig. 7).

Our results indicate that asthenosphere upwelling occurs just above the slab tearing, suggesting that the slab breach generates this upwelling. This upwelling increases the local geothermal gradient, weakening the upper plate's strength and altering the strain pattern. Consequently, strong strain gradients are expected at the edge of the asthenospheric upwelling, as evidenced by the presence of the Corinth Rift south of the slab tearing/mantle window (Fig. 7). To a lesser extent, the western rim is also associated with a strain gradient, as proposed in kinematic models (Pérouse et al., 2012) and supported by the distribution of deformation in Sporades and Thermaikos basins, where both strike-slip and extension are observed and active (Koukouvelas and Aydin, 2002; Papanikolaou et al., 2002).

The presence of a low-strength domain in North Evvia may have favoured strain localization and could have played a significant role in the propagation of the NAF, particularly for its northern and southern strands (Sengör et al., 2005). It has already been proposed that the Aegean boundary conditions, particularly the African rollback, significantly influence the extrusion of Anatolia, and the development of the NAF (Flérit et al., 2004). However, existing elastic models do not adequately account for the complex and restricted damage zone at the NAF's termination in the Sporades basins, which has been present since 3–4 Ma (Ferentinos et al., 2018; Papanikolaou et al., 2002; Caroir et al., 2024). The mantle asthenospheric window that we identify between southern Evvia and the Almiros basin creates a local weakening zone that concentrates strain and facilitates the deformation (Fig. 7). This zone acts as a focal point, affecting the propagation of the major strike-slip segments of the NAF. It prevents the NAF from reaching the nearest subduction zone, participating to a diffuse Aegean plate boundary. From our model, we propose a possible catch of the NAF by mantle processes, such as slab tearing and an associated asthenospheric upwelling. In this scenario, the current shape and location of the NAF termination could be the surface expression of the slab tearing. It would also explain the proposed coupling between the propagation of the NAF and the subduction, revealed by the existence of earthquake sequences, such as the 2008 cascade of earthquakes followed by a long episode of slow slip event (Durand et al., 2014), or the existence of pure strike-slip events in the Evvia extensional province (Sboras et al., 2025).

Our model provides, therefore, a possible cause for the kinematic reorganization of the Aegean domain in Plio-Quaternary (Pérouse et al., 2012). From the Middle Miocene to the Plio-Quaternary, African slab rollback, and Anatolia extrusion implies distributed deformation in the Aegean domain with numerous strike-slip and normal faults (Papanikolaou and Royden, 2007; Faucher et al., 2021; Brun et al., 2016). During the Plio-Quaternary period, the formation of the Corinth Rift and the arrival of the NAF near continental Greece (Armijo et al., 1996) can be linked to the onset of slab tearing and the associated asthenosphere upwelling:

- The process of slab tearing facilitates the upwelling of the asthenosphere, which weakens the upper plate. This change in rheology explains the localization of strike-slip strain along the NAF (Fig. 7).
- Additionally, slab tearing intensifies extension due to the slab rollback. The well-constrained east-west oriented edge of the slab rip located south of Evvia generates a strong north-south extension in the overlying hot lithosphere (Fig. 7). It accounts for a distributed extensional system (Corinth and Evvia rifts) located between the western end of the NAF and the Kefalonia fault.

This process provides a mechanical model to explain the Plio-Quaternary strain localization in the Aegean domain, and the formation of a diffuse plate boundary.

6. Conclusion

By integrating seismological and gravity data, we demonstrate that geophysical mantle signatures in the Aegean domain necessitate a slab tearing in the westernmost Hellenic arc combined with asthenospheric upwelling. Our model reveals a vertical, 200 km-wide slab breach localized beneath the northern part of the Evvia Gulf, initiating at approximately 120 km depth. The width of this tearing facilitates asthenospheric rise to at least 60 km and potential lateral spreading.

The location of this asthenospheric upwelling aligns with surface observations, including high heat flow and hot springs, suggesting an anomalous geotherm. The rim of the upwelling corresponds to regions of strong strain gradients, including the Corinth Rift to the south and the North Aegean Trough to the north.

We propose that the slab tearing and associated mantle processes govern upper plate strain localization. The upwelling of the asthenosphere generated by the slab tearing has driven the NAF's south-westward propagation. The encounter of the NAF tip with hotter material and the presence of the slab may have decelerated or halted its propagation, favouring more distributed extensional deformation at the surface through the Corinth and Evvia rifts system.

Our findings provide a comprehensive model that integrates geophysical observations and tectonic processes, offering new insights into the dynamic evolution of the Aegean domain.

CRediT authorship contribution statement

Clarisce Kercet: Writing – original draft, Software, Methodology, Data curation, Conceptualization. **Christel Tibéri:** Writing – review & editing, Supervision, Data curation, Conceptualization. **Frédéric Gueydan:** Writing – review & editing, Supervision, Methodology, Conceptualization. **Rodolphe Cattin:** Writing – review & editing, Methodology, Conceptualization. **Eleni Karagianni:** Writing – review & editing, Data curation.

Code availability

- Our code is available in Github repository (https://github.com/ClarieKE/Gravi_crustalroot.git)
- GEEC is an open-source Matlab code to calculate gravity and gravity gradients due to irregularly shaped body mass. This code can be

found in the public GitHub repository (<https://github.com/anitasaraswati/GEEC>)

Declaration of competing interest

The authors declare that they have no known competing financial interests or personal relationships that could have appeared to influence the work reported in this paper.

Acknowledgements

The authors express gratitude to A. Tzanis and an anonymous reviewer for their insightful reviews, which enhanced our manuscript. We also thank Alexandrine Gesret for fruitful discussions on seismological proceeding, geodynamical implications and receiver functions. C. Kercet's PhD is funded by the French ministère de l'enseignement supérieur et de la recherche. E. Karagianni thanks Erasmus for mobility funding in Geosciences Montpellier. Figures were created with Generic Mapping Tool latest version (GMT 6, [Wessel et al., 2019](#)), and QGIS software (QGIS Geographic Information System. QGIS Association, <http://www.qgis.org>).

Appendix A. Supplementary data

Supplementary data to this article can be found online at <https://doi.org/10.1016/j.tecto.2025.231025>.

Data availability

Catalogues of seismicity are available at GEIN (<https://www.gein.noa.gr/en/services-products/earthquake-catalogs/>) and ISC (<https://www.isc.ac.uk/iscgem/>), USGS (<https://www.usgs.gov/programs/earthquake-hazards/earthquakes>), and EMSC (<https://www.emsc.eu>). Teleseismic data for receiver functions are available through NOA EIDA Web services (<https://eida.gein.noa.gr>) and IRIS web service (<https://service.iris.edu>). The computed receiver functions are available on Zenodo (doi:10.5281/zenodo.15609598, <https://zenodo.org/records/15609598>). The Earth gravity model EGM2008 is available at the International Gravimetric Bureau (<https://bgi.obs-mip.fr>).ETOPO1 1 arc-minute global relief model is provided by the NOAA National Centers for Environmental information (<https://www.ncei.noaa.gov/access/metadata/landing-page/bin/iso>).

References

- Akaike, H., 1974. A new look at the statistical model identification. *IEEE Trans. Autom. Control* 19, 716–723. <https://doi.org/10.1109/TAC.1974.1100705>.
- Armijo, R., Meyer, B., King, G.C.P., Rigo, A., Papanastassiou, D., 1996. Quaternary evolution of the Corinth Rift and its implication for the late Cenozoic evolution of the Aegean. *Geophys. J. Int.* 126, 11–53. <https://doi.org/10.1111/j.1365-246X.1996.tb05264x.hal-01400415>.
- Armijo, R., Meyer, B., Hubert, A., Barka, A., 1999. Westward propagation of the North Anatolian fault into the northern Aegean: timing and kinematics. *Geology* 27, 267–270. <https://doi.org/10.1130/0091-7613>.
- Baker, C., Hatzfeld, D., Lyon-Caen, H., Papadimitriou, E., Rigo, A., 1997. Earthquake mechanisms of the Adriatic Sea and Western Greece: implications for the oceanic subduction-continental collision transition. *Geophys. J. Int.* 131, 559–594. <https://doi.org/10.1111/j.1365-246X.1997.tb06600.x>.
- Biryol, C.B., Beck, S.L., Zandt, G., Özkar, A.A., 2011. Segmented African lithosphere beneath the Anatolian region inferred from teleseismic P wave tomography. *Geophys. J. Int.* 184 (3), 1037–1057.
- Bocchini, G.M., Brüstle, A., Becker, D., Meier, T., van Keken, P.E., Ruscic, M., Papadopoulos, G.A., Rische, M., Friederich, W., 2018. Tearing, segmentation, and backstepping of subduction in the Aegean: New insights from seismicity. *Tectonophysics* 734–735, 96–118. <https://doi.org/10.1016/j.tecto.2018.04.002>.
- Briole, P., Ganias, A., Elias, P., Dimitrov, D., 2021. The GPS velocity field of the Aegean. New observations, contribution of the earthquakes, crustal blocks model. *Geophys. J. Int.* 226, 468–492. <https://doi.org/10.1093/gji/ggab089.hal-03409600>.
- Brun, J.-P., Faccenna, C., 2008. Exhumation of high-pressure rocks driven by slab rollback. *Earth Planet. Sci. Lett.* 272, 1–7. <https://doi.org/10.1016/j.epsl.2008.02.038>.
- Brun, J.P., Sokoutis, D., 2010. 45 m.y. of Aegean crust and mantle flow driven by trench retreat. *Geology* 38 (9), 815–818. <https://doi.org/10.1130/G30950.1>.
- Brun, J.-P., Sokoutis, D., 2018. Core complex segmentation in North Aegean, a dynamic view. *Tectonics* 37, 1797–1830. <https://doi.org/10.1029/2017TC004939>.
- Brun, J.-P., Faccenna, C., Gueydan, F., Sokoutis, D., Philippon, M., Kydonakis, K., Gorini, C., 2016. The two-stage Aegean extension, from localized to distributed, a result of slab rollback acceleration. *Can. J. Earth Sci.* 53 (11), 1142–1157. <https://doi.org/10.1139/cjes-2015-0203>.
- Caroir, F., Chanier, F., Gaullier, V., Sakellariou, D., Bailleul, J., Maillard, A., Paquet, F., Watremez, L., Avebuch, O., Gravelae, F., Ferrière, J., 2024. Late Quaternary deformation in the western extension of the North Anatolian Fault (North Evia, Greece): Insights from very high-resolution seismic data (WATER surveys). *Tectonophysics* 870, 230138. <https://doi.org/10.1016/j.tecto.2023.230138>.
- Chailas, S., Tzanis, A., Lagios, E., 2021. A Moho depth model for the Central and Eastern Mediterranean derived from 3D flexural model and controlled by gravity data. In: 37th General Assembly of the European Seismological Commission (ESCC2021). <https://doi.org/10.13140/RG.2.2.24313.80483>.
- Chailas, S., Tzanis, A., Krantis, H., 2022. A Comprehensive Moho Surface from Arabia to Italy Based on Gravity Data: Significance on the Geodynamic Regime. In: 16th Int. Congr. Geol. Soc. Greece, 17–19 October 2022, Patras, Greece, Bull. Geol. Soc. Greece, Sp. Publ. 10, Ext. Abs. GSG2022–404, pp. 187–188.
- Cloetingh, S., van Wees, J.D., Ziegler, P.A., Lenkey, L., Beekman, F., Tesauro, M., Förster, A., Norden, B., Kaban, M., Hardebol, N., Bonté, D., Genter, A., Guillou, Frottier, L., Ter Voorde, M., Sokoutis, D., Willingshofer, E., Cornu, T., Worum, G., 2010. Lithosphere tectonics and thermo-mechanical properties: an integrated modelling approach for Enhanced Geothermal Systems exploration in Europe. *Earth Sci. Rev.* 102, 159–206. <https://doi.org/10.1016/j.earscirev.2010.05.003>.
- Confal, J., Faccenda, M., Eken, T., Taymaz, T., 2018. Numerical simulation of 3-D mantle flow evolution in subduction zone environments in relation to seismic anisotropy beneath the eastern Mediterranean region. *Earth Planet. Sci. Lett.* 497, 50–61. <https://doi.org/10.1016/j.epsl.2018.06.005>.
- Confal, J., Bezada, M., Eken, T., Faccenda, M., Saygin, E., Taymaz, T., 2020. Influence of upper mantle anisotropy on isotropic P-wave tomography images obtained in the eastern mediterranean region. *J. Geophys. Res. Solid Earth* 125, e2019JB018559. doi:<https://doi.org/10.1029/2019JB018559>.
- Cossette, E., Audet, P., Schneider, D., Grasemann, B., 2016. Structure and anisotropy of the crust in the Cyclades, Greece, using receiver functions constrained by in situ rock textural data. *J. Geophys. Res. Solid Earth* 121, 2661–2678. <https://doi.org/10.1002/2015JB012460>.
- Cubuk-Sabuncu, Y., Taymaz, T., Fichtner, A., 2017. 3-D crustal velocity structure of western Turkey: constraints from full-waveform tomography. *Phys. Earth Planet. Inter.* 270, 90–112. <https://doi.org/10.1016/j.pepi.2017.06.014>.
- D'Alessandro, W., Brusca, L., Kyriakopoulos, K., Michas, G., Papadakis, G., 2008. Methana, the westernmost active volcanic system of the South Aegean arc (Greece): Insight from fluids geochemistry. *J. Volcanol. Geotherm. Res.* 178, 818–828. <https://doi.org/10.1016/j.jvolgeores.2008.09.014>.
- Durand, V., Bouchon, M., Floyd, M., Theodoulidis, N., Marsan, D., Karabulut, H., Schmitbuhl, J., 2014. Observation of the spread of slow deformation in Greece following the breakup of the slab. *Geophys. Res. Lett.* 41 (20), 7129–7134. <https://doi.org/10.1002/2014GL061408.hal-02323406>.
- Engdahl, E.R., van der Hilst, R., Buland, R., 1998. Global teleseismic earthquake relocation with improved travel times and procedures for depth determination. *Bull. Seismol. Soc. Am.* 88, 722–743.
- Erman, C., Yolsal-Cevikbilen, S., Eken, T., Huang, Z., Taymaz, T., 2025. Seismic anisotropy variations in the Eastern Mediterranean Sea region revealed by Splitting Intensity tomography: Implications on mantle dynamics. *J. Geophys. Res. Solid Earth* 130. <https://doi.org/10.1029/2024JB030331.e2024JB030331>.
- Evangelidis, C.P., 2017. Seismic anisotropy in the Hellenic subduction zone: effects of slab segmentation and subslab flow. *Earth Planet. Sci. Lett.* 480, 97–106. <https://doi.org/10.1016/j.epsl.2017.10.003>.
- Faccenna, C., Jolivet, L., Piromallo, C., Morelli, A., 2003. Subduction and the depth of convection in the Mediterranean mantle. *J. Geophys. Res.* 108 (B2), 2099. <https://doi.org/10.1029/2001JB001690>.
- Faucher, A., Gueydan, F., Jolivet, M., Alsaif, M., Célérier, B., 2021. Dextral strike-slip and normal faulting during middle Miocene back-arc extension and westward Anatolia extrusion in Central Greece. *Tectonics* 40. <https://doi.org/10.1029/2020TC006615.e2020TC006615>.
- Ferentinos, G., Georgiou, N., Christodoulou, D., Geraga, M., Papatheodorou, G., 2018. Propagation and termination of a strike slip fault in an extensional domain: the westward growth of the North Anatolian Fault into the Aegean Sea. *Tectonophysics* 745, 183–195. <https://doi.org/10.1016/j.tecto.2018.08.003>.
- Flérit, F., Armijo, R., King, G., Meyer, B., 2004. The mechanical interaction between the propagating North Anatolian Fault and the back-arc extension in the Aegean. *Earth Planet. Sci. Lett.* 224, 347–362. <https://doi.org/10.1016/j.epsl.2004.05.028>.
- Fullea, J., Fernandez, M., Zeyen, H., 2008. FA2BOUG – a FORTRAN 90 code to compute Bouguer gravity anomalies from gridded free-air anomalies: Application to the Atlantic-Mediterranean transition zone. *Comput. Geosci.* 34, 1665–1681. <https://doi.org/10.1016/j.cageo.2008.02.018>.
- Fytikas, M.D., Kolios, N.P., 1979. Preliminary heat flow map of Greece. In: Cermak, V., Rybach, L. (Eds.), *Terrestrial Heat Flow in Europe*. Springer Verlag, Heidelberg-Berlin-New York, pp. 197–205. https://doi.org/10.1007/978-3-642-95357-6_20.
- Galanopoulos, D., Sakkas, V., Kosmatos, D., Lagios, E., 2005. Geoelectric investigation of the Hellenic subduction zone using long period magnetotelluric data. *Tectonophysics* 409, 73–84. <https://doi.org/10.1016/j.tecto.2005.08.010>.

- Gautier, P., Brun, J.-P., Moriceau, R., Sokoutis, D., Martinod, J., Jolivet, L., 1999. Timing, kinematics and cause of the Aegean extension: a scenario based on a comparison with simple analogue experiments. *Tectonophysics* 315, 31–72.
- Govers, R., Fichtner, A., 2016. Signature of slab fragmentation beneath Anatolia from full-waveform tomography. *Earth Planet. Sci. Lett.* 450, 10–19.
- Grigoriadis, V., Tziavos, I., Tsokas, G., Stampolidis, A., 2016. Gravity data inversion for Moho depth modeling in the Hellenic area. *Pure Appl. Geophys.* 173, 1223–1241. <https://doi.org/10.1007/s00024-015-1174-y>.
- Gueydan, F., Sakellariou, D., Paquette, J.L., Roger, F., Alsaif, M., Faucher, A., Oliot, E., 2025. Late Miocene high-angle faulting in the Cyclades: offshore–onshore tectonic studies and U-Pb calcite dating. *BSGF - Earth Sci. Bull.* 196, 1. <https://doi.org/10.1051/bsgf/2024022>.
- Guillaume, B., Husson, L., Funiciello, F., Faccenna, C., 2013. The dynamics of laterally variable subductions: laboratory models applied to the Hellenides. *Solid Earth* 4, 179–200. <https://doi.org/10.5194/se-4-179-2013>.
- Gürer, D., Plunder, A., Kirst, F., Corfu, F., Schmid, S.M., van Hinsbergen, D.J.J., 2018. A long-lived late Cretaceous–early Eocene extensional province in Anatolia? Structural evidence from the İvriz Detachment, southern Central Turkey. *Earth Planet. Sci. Lett.* 481, 111–124. <https://doi.org/10.1016/j.epsl.2017.10.008>.
- Halpaap, F., Rondenay, S., Ottemöller, L., 2018. Seismicity, deformation, and metamorphism in the Western Hellenic Subduction Zone: New constraints from tomography. *J. Geophys. Res. Solid Earth* 123, 3000–3026. <https://doi.org/10.1002/2017JB015154>.
- Halpaap, F., Rondenay, S., Perrin, A., Goes, S., Ottemöller, L., Austrheim, H., Shaw, R., Eken, T., 2019. Earthquakes track subduction fluids from slab source to mantle wedge sink. *Sci. Adv.* 5, eaav7369. <https://doi.org/10.1126/sciadv.aav7369>.
- Hansen, S., Evangelidis, C., Papadopoulos, G., 2019. Imaging slab detachment within the western Hellenic Subduction Zone. *Geochem. Geophys. Geosyst.* 20, 895–912. <https://doi.org/10.1029/2018GC007810>.
- Hashida, T., Stavrakakis, G., Shimazaki, K., 1988. Three-dimensional seismic attenuation structure beneath the Aegean region and its tectonic implication. *Tectonophysics* 145, 43–54. [https://doi.org/10.1016/0040-1951\(88\)90314-9](https://doi.org/10.1016/0040-1951(88)90314-9).
- Hatzfeld, D., 1994. On the shape of the subducting slab beneath the Peloponnese, Greece. *Geophys. Res. Lett.* 21 (3), 173–176.
- Hatzfeld, D., 1999. The present-day tectonics of the Aegean as deduced from seismicity. *Geol. Soc. Lond. Spec. Publ.* 156, 415–426. <https://doi.org/10.1144/GSL.SP.1999.156.01.19>.
- Hollenstein, Ch., Müller, M.D., Geiger, A., Kahle, H., 2008. Crustal motion and deformation in Greece from a decade of GPS measurements, 1993–2003. *Tectonophysics* 449, 17–40. <https://doi.org/10.1016/j.tecto.2007.12.006>.
- Jolivet, L., Brun, J.-P., 2010. Cenozoic geodynamic evolution of the Aegean. *Int. J. Earth Sci.* 99, 109–138. <https://doi.org/10.1007/s00531-008-0366-4>.
- Jolivet, L., Faccenna, C., 2000. Mediterranean extension and the Africa-Eurasia collision. *Tectonics* 19, 1095–1106. <https://doi.org/10.1029/2000TC900018>.
- Jolivet, L., Faccenna, C., Huet, B., Labrousse, L., Le Pourhiet, L., Lacombe, O., Lecomte, E., Buoy, E., Denèle, Y., Brun, J.-P., Philippot, M., Paul, A., Salaün, G., Karabulut, H., Piromallo, C., Monié, P., Gueydan, F., Okay, A., Oberhänsli, R., Pourteau, A., Augier, R., Gadenne, L., Driussi, O., 2013. Aegean tectonics: Strain localisation, slab tearing and trench retreat. *Tectonophysics* 597–598, 1–33. <https://doi.org/10.1016/j.tecto.2012.06.011>.
- Jolivet, L., Menant, A., Sternai, P., Rabillard, A., Arbaret, L., Augier, R., Laurent, V., Beaudouin, A., Grasemann, B., Huet, B., Labrousse, L., Le Pourhiet, L., 2015. The geological signature of a slab tear below the Aegean. *Tectonophysics* 659, 166–182. <https://doi.org/10.1016/j.tecto.2015.08.004>.
- Karagianni, E., Papazachos, C.B., Panagiotopoulos, D.G., Suhadolc, P., Yuan, A., Panza, G.F., 2005. Shear velocity structure in the Aegean area obtained by inversion of Rayleigh waves. *Geophys. J. Int.* 160, 127–143. <https://doi.org/10.1111/j.1365-246X.2005.02354.x>.
- Kassaras, I., Kapetanidis, V., Karakontstantis, A., Papadimitriou, P., 2020a. Deep structure of the Hellenic lithosphere from teleseismic Rayleigh-wave tomography. *Geophys. J. Int.* 221, 205–230. <https://doi.org/10.1093/gji/ggz579>.
- Kassaras, I., Kapetanidis, V., Chailas, S., Kouskouna, V., Papadimitriou, P., 2020b. The new seismotectonic atlas of Greece (v1.0) and its implementation. *Geosciences* 10, 447. <https://doi.org/10.3390/geosciences10110447>.
- Kennett, B., Engdahl, E., 1991. Traveltimes for global earthquake location and phase identification. *Geophys. J. Int.* 105, 429–465. <https://doi.org/10.1111/j.1365-246X.1991.tb06724.x>.
- Koukouvelas, I., Aydin, A., 2002. Fault structure and related basins of the North Aegean Sea and its surroundings. *Tectonics* 21, 1046. <https://doi.org/10.1029/2001TC001037>.
- Lagios, E., Chailas, S., Hipkin, R.G., 1996. Newly compiled gravity and topographic data banks of Greece. *Geophys. J. Int.* 126 (1), 287–290. <https://doi.org/10.1111/j.1365-246X.1996.tb05287.x>.
- Le Pichon, X., Angelier, J., 1979. The Hellenic arc and the trench system: a key to the neotectonic evolution of the eastern Mediterranean area. *Tectonophysics* 60, 1–42.
- Le Pichon, X., Chamot-Rooke, N., Rangin, C., Şengör, A.M.C., 2003. The North Anatolian fault in the Sea of Marmara. *J. Geophys. Res.* 108, 2179. <https://doi.org/10.1029/2002JB001862>.
- Ligorria, J., Ammon, C., 1999. Iterative deconvolution and receiver function estimation. *Bull. Seismol. Soc. Am.* 89, 1395–1400. <https://doi.org/10.1785/bssa0890051395>.
- Lundgren, P., Giardini, D., Russo, R.M., 1998. A geodynamic framework for eastern Mediterranean kinematics. *Geophys. Res. Lett.* 25, 4007–4010.
- Makris, J., Papoulia, J., Yegorova, T., 2013. A 3-D density model of Greece constrained by gravity and seismic data. *Geophys. J. Int.* 194, 1–17. <https://doi.org/10.1093/gji/ggt059>.
- Makropoulos, K., Burton, P., 1981. A catalogue of seismicity in Greece and adjacent areas. *Geophys. J. R. Astron. Soc.* 65, 741–762.
- Meier, T., Rische, M., Endrun, B., Vafidis, A., Harjes, H.-P., 2004. Seismicity of the Hellenic subduction zone in the area of western and Central Crete observed by temporary local seismic networks. *Tectonophysics* 383, 149–169. <https://doi.org/10.1016/j.tecto.2004.02.004>.
- Michailos, K., Hetényi, G., Scarponi, M., Stipčević, J., Bianchi, I., Bonatto, L., Czuba, W., Di Bona, M., Govoni, A., Hannemann, K., Janik, T., Kalmár, D., Kind, R., Link, F., Lucente, F.P., Monna, S., Montuori, C., Mroczek, S., Paul, A., Piromallo, C., Plomerová, J., Rewers, J., Salimbeni, S., Tilman, F., Środa, P., Vergne, J., the AlpArray-PACASE Working Group, 2023. Moho depths beneath the European Alps: a homogeneously processed map and receiver functions database. *Earth Syst. Sci. Data*. 15, 2117–2138. <https://doi.org/10.5194/essd-15-2117-2023>.
- Olive, J.-A., Pearce, F., Rondenay, S., Behn, M., 2014. Pronounced zonation of seismic anisotropy in the Western Hellenic subduction zone and its geodynamic significance. *Earth Planet. Sci. Lett.* 391, 100–109. <https://doi.org/10.1016/j.epsl.2014.01.029>.
- Papanikolaou, D., 2013. Tectonostratigraphic models of the Alpine terranes and subduction history of the Hellenides. *Tectonophysics* 595–596, 1–24. <https://doi.org/10.1016/j.tecto.2012.08.008>.
- Papanikolaou, D., Royden, L., 2007. Disruption of the Hellenic arc: late Miocene extensional detachment faults and steep Pliocene–Quaternary normal faults – or what happened at Corinth? *Tectonics* 26, TC5003. <https://doi.org/10.1029/2006TC002007>.
- Papanikolaou, D., Alexandri, M., Nomikou, P., Ballas, D., 2002. Morphotectonic structure of the western part of the North Aegean Basin based on swath bathymetry. *Mar. Geol.* 190, 465–492. [https://doi.org/10.1016/S0025-3227\(02\)00359-6](https://doi.org/10.1016/S0025-3227(02)00359-6).
- Papazachos, B.C., 1990. Seismicity of the Aegean and surrounding area. *Tectonophysics* 178, 287–308.
- Papazachos, B.C., Karakostas, V.G., Papazachos, C.B., Scordilis, E.M., 2000. The geometry of the wadati–Benioff zone and lithospheric kinematics in the Hellenic arc. *Tectonophysics* 319, 275–300. [https://doi.org/10.1016/S0040-1951\(99\)00299-1](https://doi.org/10.1016/S0040-1951(99)00299-1).
- Pavlis, N., Kenyon, S., Factor, J., Holmes, S., 2008. Earth Gravitational model 2008, SEG Technical Program Expanded Abstracts: 761–763. <https://doi.org/10.1190/1.3063757>.
- Pearce, F.D., Rondenay, S., Sachpazi, M., Charalampakis, M., Royden, L.H., 2012. Seismic investigation of the transition from continental to oceanic subduction along the western Hellenic Subduction Zone. *J. Geophys. Res.* 117, B07306. <https://doi.org/10.1029/2011JB009023>.
- Pe-Piper, G., Piper, D.J.W., 2005. The South Aegean active volcanic arc: relationships between magmatism and tectonics. In: Fytikas, M., Vougioukalakis, E. (Eds.), *Developments in Volcanology*, vol. 7, pp. 113–133. [https://doi.org/10.1016/S1871-644X\(05\)80034-8](https://doi.org/10.1016/S1871-644X(05)80034-8).
- Pe-Piper, G., Piper, D.J.W., 2007. Neogene backarc volcanism of the Aegean: New insights into the relationship between magmatism and tectonics. In: Beccaluva, L., Bianchini, G., Wilson, M. (Eds.), *Cenozoic Volcanism in the Mediterranean Area*, vol. 418. *Geol. Soc. Am. Spec. Pap.* 17–32.
- Pérōuse, E., Chamot-Rooke, N., Rabautte, A., Briole, P., Jouanne, F., 2012. Bridging onshore and offshore present-day kinematics of central and eastern Mediterranean: Implications for crustal dynamics and mantle flow. *Geochem. Geophys. Geosyst.* 13 (9), 1–13. <https://doi.org/10.1029/2012GC004289>, hal-01438195.
- Pik, R., Marty, B., 2009. Helium isotopic signature of modern and fossil fluids associated with the Corinth rift fault zone (Greece): implication for fault connectivity in the lower crust. *Chem. Geol.* 266, 67–75. <https://doi.org/10.1016/j.chemgeo.2008.09.024>.
- Piromallo, C., Morelli, A., 2003. P wave tomography of the mantle under the Alpine–Mediterranean area. *J. Geophys. Res.* 108, 2065. <https://doi.org/10.1029/2002JB001757>.
- Portner, D.E., Delph, J.R., Biryol, C.B., Beck, S.L., Zandt, G., Özcar, A.A., Sandvol, E., Türkelli, N., 2018. Subduction termination through progressive slab deformation across Eastern Mediterranean subduction zones from updated P-wave tomography beneath Anatolia. *Geosphere* 14 (3), 907–925. <https://doi.org/10.1130/GES01617.1>.
- Ranjan, P., Konstantinou, K.I., 2024. Local earthquake tomography of the Aegean crust: Implications for active deformation, large earthquakes, and arc volcanism. *Tectonophysics* 880, 230331. <https://doi.org/10.1016/j.tecto.2024.230331>.
- Ranjan, P., Stehly, L., 2024. Estimation of seismic attenuation from ambient noise coda waves: application to the Hellenic subduction zone. *Bull. Seismol. Soc. Am.* 114, 2065–2082. <https://doi.org/10.1785/0120230265>, HAL:insu-04836698.
- Rappisi, F., Lo Bue, R., Vanderbeek, B.P., Confal, J.M., Erman, C., Baccheschi, P., Pondrelli, S., Eken, T., Yolsal-Çevikbilek, S., Faccenda, M., 2025. 3-D mantle flow and structure of the Mediterranean from combined P-wave and splitting intensity anisotropic tomography. *J. Geophys. Res. Solid Earth* 130, e2024JB030883. <https://doi.org/10.1029/2024JB030883>.
- Reilinger, R., McClusky, S., Paradissis, D., Ergintav, S., Vernant, P., 2010. Geodetic constraints on the tectonic evolution of the Aegean region and strain accumulation along the Hellenic subduction zone. *Tectonophysics* 488, 22–30. <https://doi.org/10.1016/j.tecto.2009.05.027>.
- Roche, V., Jolivet, J., Papanikolaou, D., Bozkurt, E., Menant, A., Rimmelé, G., 2019. Slab segmentation beneath the Aegean/Anatolia transition zone: insights from the tectonic and metamorphic evolution of the Eastern Aegean region. *Tectonophysics* 754, 101–129. <https://doi.org/10.1016/j.tecto.2019.01.016>.
- Rodriguez, M., Sakellariou, D., Gorini, C., Janin, A., D'Acremont, E., Le Pourhiet, L., Chamot-Rooke, N., Tsampouraki-Kraounaki, K., Morfis, I., Rousakis, G., Henry, P., Lurin, A., Delescluse, M., Briole, P., Rigo, A., Arsenikos, S., Bulois, C., Fernández-Blanco, D., Beniest, A., Grall, C., Chanier, F., Caroir, F., Dessa, J.-X., Oregoni, D., Nercessian, A., 2023. Evolution of the North Anatolian Fault from a diffuse to a

- localized shear zone in the North Aegean Sea during the Plio-Pleistocene. *Geophys. J. Int.* 235, 2614–2639. <https://doi.org/10.1093/gji/ggd364>.
- Rondenay, S., 2006. Multi-disciplinary experiments for Dynamic Understanding of Subduction under the Aegean Sea [dataset]. Intern. Feder. Digi. Seismogr. Network. https://doi.org/10.7914/SN/XS_2006.
- Royden, L.H., 1993. Evolution of retreating subduction boundaries formed during continental collision. *Tectonics* 12, 629–638. <https://doi.org/10.1029/92TC02641>.
- Royden, L.H., Papanikolaou, D., 2011. Slab segmentation and late Cenozoic disruption of the Hellenic arc. *Geochem. Geophys. Geosyst.* 12, Q03010. <https://doi.org/10.1029/2010GC003280>.
- Sachpazi, M., Laigle, M., Charalampakis, M., Sakellariou, D., Flueh, E., Sokos, E., Daskalaki, E., Galv  , A., Petrou, P., Hirn, A., 2016. Slab segmentation controls the interplate slip motion in the SW Hellenic subduction: New insight from the 2008 Mw 6.8 Methoni interplate earthquake. *Geophys. Res. Lett.* 43, 9619–9626. <https://doi.org/10.1002/2016GL070447>.
- Sakellariou, D., Tsampouraki-Kraounaki, K., 2018. Plio-Quaternary extension and strike-slip tectonics in the Aegean. In: Duarte, J. (Ed.), *Transform Plate Boundaries and Fracture Zones*. Elsevier.
- Salau  n, G., Pedersen, H., Paul, A., Farra, V., Karabulut, H., Hatzfeld, D., Papazachos, C., Childs, D., Pequegnat, C., SIMBAAD Team, 2012. High-resolution surface wave tomography beneath the Aegean-Anatolia region: constraints on upper-mantle structure. *Geophys. Int. J.* 190, 406–420. <https://doi.org/10.1111/j.1365-246X.2012.05483.x>.
- Sarawati, A., Cattin, R., Mazotti, S., Cadio, C., 2019. New analytical solution and associated software for computing full-tensor gravitational field due to irregularly shaped bodies. *J. Geodyn.* 93, 1–17. <https://doi.org/10.1007/s00190-019-01309-y>.
- Sboras, S., Mouzakiotis, E., Chousianitis, K., Karastathis, V., Evangelidis, C., Lazos, I., Papageorgiou, A., Liakopoulos, S., Iordanidou, K., 2025. Where does the active North Aegean Sea shear stop? Geodynamic and seismotectonic implications from recent strike-slip earthquake occurrences and GPS-based geodetic analysis in Euboea, Phthiotis and Boeotia, Central Greece. *Tectonophysics* 914, 230917. <https://doi.org/10.1016/j.tecto.2025.230917>.
- Seng  r, A.M.C., 1979. The North Anatolian transform fault: its age, offset and tectonic significance. *J. Geol. Soc. Lond.* 136, 269–282.
- Seng  r, A.M.C.,   zeren, S., Gen  , T., Zor, E., 2003. East Anatolian high plateau as a mantle-supported, north-south shortened domal structure. *Geophys. Res. Lett.* 30, 8045. <https://doi.org/10.1029/2003GL017858>.
- Seng  r, A.M.C., T  ysiz, O., Imre, C., Sakinc, M., Eyidogan, H., G  rtur, N., Le Pichon, X., Rangin, C., 2005. The North Anatolian Fault: a new look. *Annu. Rev. Earth Planet. Sci.* 33, 37–112. <https://doi.org/10.1146/annurev.earth.32.101802.120415>.
- Sodoudi, F., Kind, R., Hatzfeld, D., Priestley, K., Hanka, W., Wylegalla, K., Stavrakakis, G., Vafidis, A., Harjes, H.-P., Bohnhoff, M., 2006. Lithospheric structure of the Aegean obtained from P and S receiver functions. *J. Geophys. Res.* 111, B12307. <https://doi.org/10.1029/2005JB003932>.
- Sternai, P., Menant, A., Jolivet, L., Gerya, T., 2014. Subduction and mantle flow driving surface deformation in the Aegean-Anatolian system. *Earth Planet. Sci. Lett.* 405, 110–118. <https://doi.org/10.1016/j.epsl.2014.1008.1023>.
- Stiros, S.C., 1991. Heat Flow and thermal Structure of the Aegean Sea and the Southern Balkans. In: Cerm  k, V., Rybach, L. (Eds.), *Terrestrial Heat Flow and the Lithosphere Structure. Exploration of the Deep Continental Crust*. Springer, Berlin, Heidelberg. https://doi.org/10.1007/978-3-642-75582-8_19.
- Subedi, S., Het  nyi, G., Vergne, J., Bollinger, L., Lyon-Caen, H., Farra, V., et al., 2018. Imaging the Moho and the Main Himalayan Thrust in Western Nepal with receiver functions. *Geophys. Res. Lett.* 45, 13,222–13,230. <https://doi.org/10.1029/2018GL080911>.
- Suckale, J., Rondenay, S., Sachpazi, M., Charalampakis, M., Hosa, A., Royden, L.H., 2009. High-resolution seismic imaging of the western Hellenic subduction zone using teleseismic scattered waves. *Geophys. J. Int.* 178, 775–791. <https://doi.org/10.1111/j.1365-246X.2009.04170.x>.
- Taymaz, T., Jackson, McKenzie, D., 1991. Active tectonics of the north and Central Aegean Sea. *Geophys. J. Int.* 106, 433–490. <https://doi.org/10.1111/j.1365-246X.1991.tb03906.x>, hal-01400404.
- Taymaz, T., Jackson, J., Westaway, R., 1990. *Earthquake mechanisms in the Hellenic Trench near Crete*. *Geophys. J. Int.* 102, 695–731.
- Tirel, C., Gueydan, F., Tiberti, C., Brun, J.-P., 2004. Aegean crustal thickness inferred from gravity inversion: Geodynamical implications. *Earth Planet. Sci. Lett.* 228, 267–280. <https://doi.org/10.1016/j.epsl.2004.10.023>.
- Tsokas, G.N., Hansen, R.O., 1997. Study of the crustal thickness and the subducting lithosphere in Greece from gravity data. *J. Geophys. Res.* 102, 585–597. <https://doi.org/10.1029/97JB00730>.
- Tzanis, A., Chailas, S., Sagredou, M., 2022. The North Euboea (Greece) volcanic field as outlined by its Magnetic Anomalies. In: 16th Int. Congress Geol. Soc. Greece, 17–19 October 2022, Patras, Greece. *Bull. Geol. Soc. Greece, Sp. Publ.*, 10, Ext. Abs. GSG2022–245.
- U.S. Geological Survey, 2025. Earthquake Lists, Maps, and Statistics. <https://earthquake.usgs.gov/earthquakes/search/>.
- Uieda, L., Barbosa, V., 2017. Fast nonlinear gravity inversion in spherical coordinates with application to the South American Moho. *Geophys. J. Int.* 208 (1), 162–176. <https://doi.org/10.1093/gji/ggw390>.
- Uieda, L., Oliveira Jr., V.C., Barbosa, V.C.F., 2013. Modeling the Earth with Fatiando a Terra, Proceedings of the 12th Python in Science Conference, pp. 91–98. <https://doi.org/10.25080/Majora-8b375195-010>.
- Vougioukalakis, G.E., Satow, C.G., Druitt, T.H., 2019. Volcanism of the South Aegean Volcanic Arc. *Elements* 15, 159–164. <https://doi.org/10.2138/elements.15.3.159>, hal-02153654.
- Wessel, P., Luis, J.F., Uieda, L., Scharroo, R., Wobbe, F., Smith, W.H.F., Tian, D., 2019. The generic mapping tools version 6. *Geochem. Geophys. Geosyst.* 20 (11), 5556–5564. <https://doi.org/10.1029/2019GC008515>.
- Wortel, M.J.R., Spakman, W., 2000. Subduction and slab detachment in the Mediterranean-Carpathian region. *Science* 290, 1910–1917. <https://doi.org/10.1126/science.290.5498.1910>.
- Yolsal-Çevikbilen, S., Taymaz, T., 2012. Earthquake source parameters along the Hellenic subduction zone and numerical simulations of historical tsunamis in the Eastern Mediterranean. *Tectonophysics* 536–537, 61–100. <https://doi.org/10.1016/j.tecto.2012.02.019>.
- Yuan, X., Ni, J., Kind, R., Mechie, J., Sandvol, E., 1997. Lithospheric and upper mantle structure of southern Tibet from a seismological passive source experiment. *J. Geophys. Res.* 102, 27491–27500. <https://doi.org/10.1029/97JB02379>.